AIP Advances

Anisotropic wetting and final shape of droplets impacting on micropillars with non-vertical lateral walls

Wenwu Ding, Carlos A. Dorao and Maria Fernandino

View Online   **Export Citation**   **CrossMark**

AIP Advances

Call For Papers!

SPECIAL TOPIC: Advances in Low Dimensional and 2D Materials

Anisotropic wetting and final shape of droplets impacting on micropillars with non-vertical lateral walls

View Online   Export Citation   CrossMark

Wenwu Ding, (ID) **Carlos A. Dorao,** (ID) **and Maria Fernandino**[a] (ID)

AFFILIATIONS

Department of Energy and Process Engineering, Norwegian University of Science and Technology, Trondheim, Norway

[a]Author to whom correspondence should be addressed: maria.fernandino@ntnu.no

ABSTRACT

The control of the droplet shape during the impact on a solid surface is of relevance for several practical applications, such as inkjet printing technologies. Although several studies have reported factors affecting the final droplet shape, understanding of the liquid spreading process is still lacking. In this work, droplets of different velocities are deposited on surfaces patterned with conical and cylindrical pillars. It is shown that for the structures of the same height and pitch, the shape of the lateral wall of the micro-structures affects the droplet shape. In addition, at higher deposition velocity, the initial polygonal/square shape of the droplets evolves into a more circular shape. The change in the shape due to the lateral wall of the structures is the result of the solid–liquid contact both above and below the structures and the way in which the liquid is able to move in between the structures for different passage areas.

I. INTRODUCTION

Structured surfaces have been the focus of research during the last few years as a way to manipulate wetting properties[1,2] in applications where droplet manipulation is important, such as inkjet printing,[3–6] liquid metal printing,[7,8] and solder droplet printing.[9,10] It is well known that droplets deposited on rough patterned surfaces can attain different shapes.[11] When the droplet is in the Cassie state, the droplet shows a high apparent contact angle and a circular shape. However, with decreasing surface tension, a droplet can penetrate into the structure, resulting in a Wenzel state droplet where different shapes can be observed.[11–14] Manipulation of the shape is especially useful for various printing applications, such as inkjet printing,[3–6] liquid metal printing,[7,8] and solder droplet printing.[9,10] The physics behind the various factors is mainly ascribed to how liquid evolves during the spreading process.[11,13,17–19] Mainly, the heterogeneity in

Several factors have been reported to affect the droplet shape, including the square or hexagonal pattern arrangement,[12,14] structure design parameters such as height-to-pitch ratio,[13] droplet surface tension and equilibrium contact angle,[13] symmetry and spacing of the pillar lattice and shape of the top of the pillars,[11,14] structure diameter-to-pitch ratio,[11] and droplet composition.[15,16] The physics behind the various factors is mainly ascribed to how liquid evolves during the spreading process.[11,13,17–19] Mainly, the heterogeneity in

the droplet shape depends on the different spreading velocities along the normal and diagonal directions with respect to the row of pillars, as a result of the balance between capillary and viscous forces[13] and excess driving energy and resistance induced by the micropillars.[17] At the same time, Raj *et al.*[11] proposed that the various shapes are due to the difference in the advancing contact angle in the axial and diagonal directions. Pinning of the contact line has also been assigned an important role in influencing the final droplet shape.[13,14] In addition, the spreading process is affected by the wetting transition behavior.[19] While all the previous studies involved pillars of different shapes and geometrical arrangements, none of them considers structures with different lateral wall shapes. Given that capillary and viscous forces and pinning effects are the ones determining the final droplet shape, it can be expected that different lateral wall shapes of the surface structures have an influence on the spreading of the liquid and thus the final droplet shape.

As opposed to droplets being gently deposited on a surface, many applications, such as inkjet printing where droplet shape manipulation is important, involve droplets reaching the surface at finite speeds. Anisotropic wetting during the droplet impact on micro-structured surfaces has been investigated in the literature both numerically[20,21] and experimentally.[22–27] When the roughness

geometry is not isotropic, the apparent contact angle is found to be different in different directions. This difference has been attributed to the pinning of the contact line on the top of the pillars during the impact on hydrophobic parallel grooves.[20,26] This pinning of the contact line enhanced the anisotropy of the droplet shape, which was seen to increase with the increasing impact We number.[25,26] Faceted droplets during the impact on superhydrophobic pillar arrangements have been explained by the partial penetration of the liquid into the structures for larger We numbers[22,23] and by the capillary and viscous forces retarding the movement of the contact line in different directions between adjacent pillars.[24,27] All these droplet impact studies have been performed on superhydrophobic surfaces with microstructures with vertical lateral walls, where both Cassie and Wenzel wetting states were observed.

In this study, we investigate the effect of a non-vertical lateral wall of the microstructures on the droplet shape during the impact on surfaces, showing only the Wenzel wetting state. We use truncated conical pillars to demonstrate that the side wall shape of the surface structures affects the spreading velocity of the liquid in different directions, thus influencing the final droplet shape. Droplets are released from different heights and impact the structured surface with velocity ranging from 0.4 to 1.7 m/s. In addition to the shape of the lateral wall of structures, both the pitch distance of the microstructures and impacting velocity can be used to control the final droplet shape.

II. EXPERIMENTAL

The samples, a syringe, an x–y moving stage, a vertical moving stage, a digital microscope (Keyence, VHX-950F), and a microscope stage were placed as shown in Fig. 1 for top view imaging. The sample was placed on the x–y moving stage initially below the syringe, which, in turn, was mounted on a vertical stage that can be moved up and down to adjust the deposition height. After a single droplet was produced from the syringe and deposited on the sample, the sample was moved in order to have the droplet below the microscope lens, and the top view image of the droplet shape was recorded.

Structured surfaces with a square arrangement of cylindrical or conical pillars are produced using photolithography and dry etching techniques as schematically shown in Fig. 2. First, the silicon wafer is rinsed with the solvent, acetone, ethanol, isopropanol, and deionized water. The wafer is then dried with N$_2$ gas. Next, we coat the sample with negative photoresist Mr-dwl-5 at 3000 rpm for 30 s and prebake the sample. The desired pattern is transferred by exposing the sample with a 405 nm wavelength laser using a MLA150
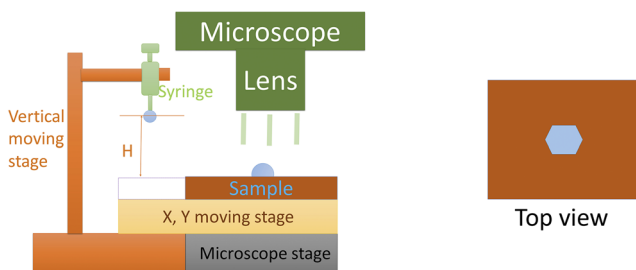

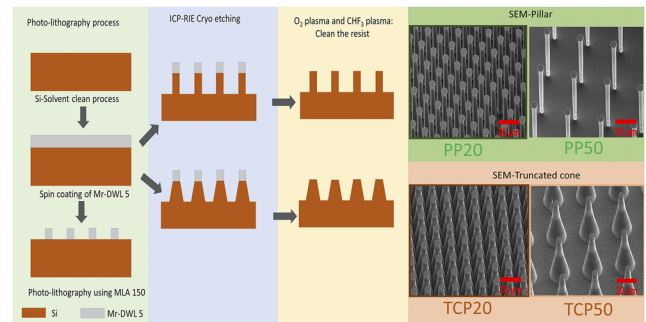**FIG. 1.** Schematic illustration of the experimental setup used in this study.

FIG. 2. Schematic demonstration of the sample fabrication process and SEM picture of produced samples.

TABLE I. Samples used in this study. Nomenclature used for sample names (e.g., TCP20H40)—TC: truncated cone; P: cylindrical pillar; Pxx: pitch; and Hxx: height.

Sample name	Pillar shape	Pitch (μm)	Height (μm)
TCP20H40	Conical	20	40
TCP30H40	Conical	30	40
TCP50H40	Conical	50	40
TCP70H33	Conical	70	33
PP20H40	Cylindrical	20	40
PP30H40	Cylindrical	30	40
PP50H40	Cylindrical	50	40

(Heidelberg Instruments). After development in Mr dev 600, the silicon wafer is patterned with a square arrangement of circles 10 μm in diameter and a pitch of 20, 30, or 50 μm. An Oxford Cryo ICP-RIE dry etching device is utilized to perform plasma etching of the samples using SF$_6$/O$_2$ and CHF$_3$. For the case of conical pillars, the etching was performed at −80 Celsius degrees, with SF$_6$/O$_2$-85/16 SCCM, at a pressure of 42 mTorr during 23 min, followed by O$_2$ plasma during 15 min and CHF$_3$ plasma for 5 min. For the cylindrical pillars, etching was performed at −100 Celsius degrees, with SF$_6$/O$_2$-100/11 SCCM at a pressure of 20 mTorr during 29 min, followed by O$_2$ plasma during 15 min and CHF$_3$ plasma for 5 min. After etching, samples are cleaned with an oxygen plasma in order to remove any remaining photoresist. Since after oxygen treatment the samples can show the aging effect, namely, change in the intrinsic contact angle with time,[28] the samples are further exposed to a silane [trichloro(1H,1H,2H,2H-perfluorooctyl)silane, Sigma-Aldrich] atmosphere for 3 h. In this way, the samples did not show any change in intrinsic wetting properties during the whole study. Different types of surface topologies are obtained by using different etching parameters. Examples of produced surfaces are shown in the scanning electron microscopy (SEM) images in Fig. 2. Table I presents a list of the fabricated surfaces and the geometrical properties of the structures.

III. RESULTS AND DISCUSSION

Three mixtures of ethanol and DI water were used in this study. The mixture composition, surface tension, and equilibrium contact angle can be found in Table II. The different mixture compositions were chosen so as to have different surface tensions (i.e., the effect of

TABLE II. Ethanol/DI water mixtures used in this study.

Liquid	Surface tension (mN/m)	Intrinsic angle (deg)
67 vol. % ethanol/DI water	27 ± 1	55 ± 5
35 vol. % ethanol/DI water	33 ± 1	63 ± 3
23 vol. % ethanol/DI water	37 ± 1	74 ± 4

capillary force on the observed phenomena) while keeping the surface tension in the range where Wenzel-state droplets were obtained on the tested surfaces (before getting into the hemi-wicking range) for the purposes of this study. The surface tension of the mixtures was measured by using the pendant drop method. The static contact angle of the mixtures was measured with an optical tensiometer and corresponds to the intrinsic equilibrium contact angle for the considered surfaces, i.e., contact angle on a flat silicon surface covered with the same silane treatment as the structured sample.

It is known that concentration gradient driven phenomena can affect the droplet behavior on a surface through internal Marangoni flow re-circulations and earlier depinning of the contact line due to the faster evaporation of the more volatile component.[15] However, the volume of the droplet lying on the surface changed by less than 5% in 10 s, more time than it took us to take the pictures of the droplet. In addition, we did not observe any change in the droplet during this 10 s. Therefore, concentration effects were considered negligible during this study.

A droplet lying on an ordered patterned of pillars will spread with different velocities in the direction normal to the pillar rows and along the diagonal direction. Depending on this difference in velocity, the droplet can attain either a circular or non-circular shape, such as an octagon or a square. The different spreading velocity in each direction is attributed to the balance between capillary and viscous forces[13,29] and contact line pinning effects.[11,14] In particular, the study by Courbin et al.[13] showed that the final shape of the droplet on a square arrangement of cylindrical pillars depends on the height-to-pitch ratio (H/P) of the structures and on the liquid surface tension. However, if the difference in spreading velocity depends on capillary forces, it can be expected that the lateral shape of the pillars also has an important role.

Here, we deposited a droplet on a square array of cylindrical and conical pillars with the same height (40 μm) and two different pitch distances, namely, 20 and 50 μm. The results after the droplets have achieved a steady shape and position can be seen in Fig. 3. For a pitch of 20 μm, the droplet on the conical pillars shows a slightly octagonal shape, while the droplet on the cylindrical pillars is clearly a square. As the pitch is increased to 50 μm, the droplet on the conical pillars evolves into a more clear octagon, whereas the droplet on the cylindrical pillars tends toward a circular shape. Since the top of both types of structures is the same for a constant H/P and surface tension values, these results clearly show that the lateral walls of the pillars play an important role in the speed of spreading of the liquid in different directions.

In the case of cylindrical pillars [Fig. 3(b)], going from a square-shaped droplet to a rounded one when the pillar density (i.e., diameter-to-pitch ratio) is decreased is in agreement with the previously reported results.[11,14] This phenomenon has been attributed to the change in the local contact angle due to different energy barriers for local depinning of the contact line in the normal and diagonal directions to the pillar rows. It has been shown that by changing the shape of the top of the pillars, the depinning of the contact line can be favored, thus obtaining different droplet shapes for the same lattice arrangement.[14] Figure 4 shows the top view images of a droplet of the 67 vol. % ethanol/DI-water mixture expanding on cylindrical pillar surfaces for two different pitches while the liquid is being injected into the existing droplet. For a pitch of 20 μm, the liquid moves mainly in the diagonal direction with respect to the row of pillars, which will end up in a squared-shape droplet as shown in Fig. 3(a). When the pitch is increased to 50 μm, the liquid movement is similar in both the normal and diagonal directions to the row of pillars, resulting in a more circular droplet.
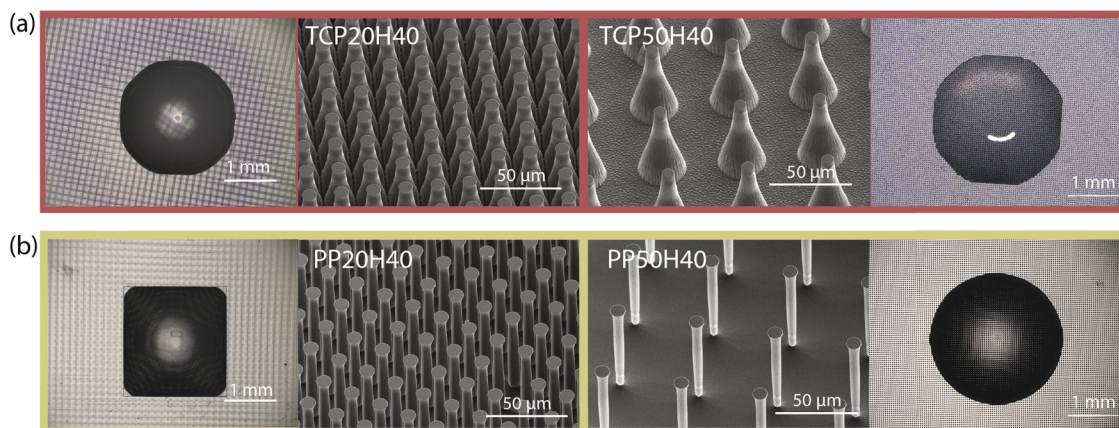

FIG. 3. Droplet with surface tension γ = 27 mN/m deposited from a height of 2 cm (We = 12) on (a) conical pillars with a pitch of 20 μm (left) and 50 μm (right) and on (b) cylindrical pillars with a pitch of 20 μm (left) and 50 μm (right).
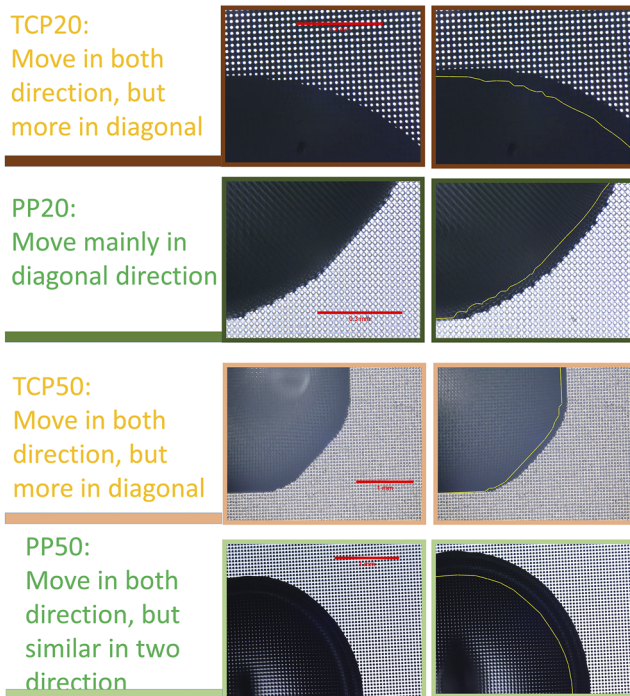
FIG. 4. Liquid spreading recorded around the droplet corner region while injecting liquid into the existing droplet. The liquid surface tension was γ = 27 mN/m. For a pitch of 20 μm, the cylindrical pillar surface shows more movement in the diagonal direction as compared to the normal direction to the row of pillars. For the truncated cone structures, similar liquid spreading is observed in both directions. At a pitch of 50 μm, the cylindrical pillar surface shows similar liquid movement in the two directions, while the truncated cone surface shows more movement in the diagonal direction.

FIG. 5. Liquid advancing from one conical pillar row to the next one. The liquid reaches the next row of conical pillars traveling along the bottom surface first. Once the new row is reached, the rest of the liquid moves above the structures until the liquid covers the top of the whole conical structures. The cycle begins again with the liquid remaining on the top of the cones and advancing to the next row along the surface bottom.

For the conical pillars in Fig. 3(a), the droplet shape is slightly octagonal and almost circular for both tested pitches. This indicates a similar spreading velocity both in the normal and diagonal directions. The top of the structures of the truncated conical and cylindrical pillars is identical, implying that the local pinning of the contact line at the top of the structures is similar in both directions. The difference in the behavior of the droplet on the conical pillars with respect to the one on cylindrical pillars is therefore attributed to the inclination of the lateral wall of the structures.

Figure 5 shows the snapshots of the liquid spreading over conical pillars and a schematic representation of the process. Different from what happens for cylindrical pillars, the liquid does not seem to be pinned on the top of the structures but rather around the cones pinned on their baseline, with liquid covering the top of the structures (left pictures in Fig. 5). The contact angle will then increase until it reaches the value corresponding to the local advancing angle for the inclined lateral wall, the point at which the liquid will start descending along this wall and coming over the next ascending one due to capillary forces. Once the liquid advances along the lateral wall, the spreading velocity will be determined by the balance of capillary and viscous forces. When the liquid reached the next row, it covers the top of these structures and starts to advance along the inclined walls surrounding each cone.
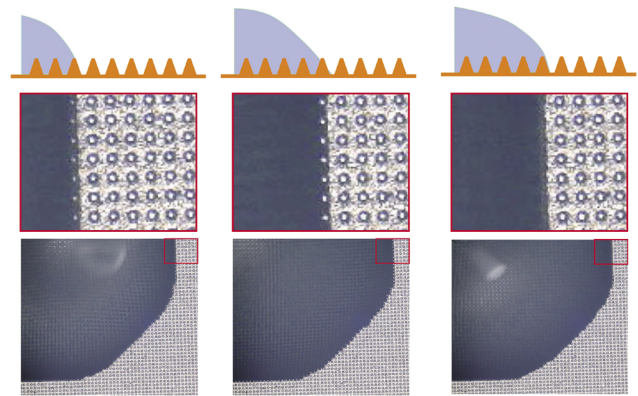
Depending on the advancing direction (normal or diagonal to the row of structures), the liquid will face a different cross-sectional area to flow into. For cylindrical pillars, the liquid will advance along a flat bottom with vertical lateral walls that have a certain distance apart until reaching the next row of pillars. The velocity of the contact line will depend on the ability of the liquid to advance to the next row of structures along this flat bottom.[13] The distance between the adjacent lateral pillars will be different when coming along the normal or diagonal direction, i.e., a different line of sight when moving in the normal or diagonal direction. For the conical pillars, the liquid will see a triangular-shaped cross section, with less difference between diagonal and normal directions, and in particular no flat bottom. This will result in a similar spreading velocity in each direction and therefore a more homogeneous droplet shape. As the conical pillars get further away from each other, their bases will no longer be in contact and a flat bottom surface will begin to appear. In this case, it is expected that the liquid spreading velocity will be more similar to the case of cylindrical pillars.

Since the less heterogeneous shape of the droplets on conical pillars is attributed to the inclined lateral wall of the structures, we varied the pitch of the structures (while keeping their height constant) to see the behavior of the droplets in the limit when the conical pillars get closer to a cylindrical pillar arrangement. Figure 6 shows how the droplet becomes more circular both for cylindrical and conical pillars for larger pitch distances. As the pitch increases, the liquid advancing from one row of cones to the next ones has a line of sight more similar to the case of the adjacent row of cylindrical pillars, i.e., almost vertical walls with a flat bottom. Still, for a pitch of 50 μm, the droplet on the truncated cones is not completely circular. This is attributed to the fact that the lateral walls of the conical pillars provide an extra surface for the liquid to creep to the next row of structures much sooner than for the cylindrical pillars with the same pitch. Looking at the truncated cone sample with a pitch of 50 μm in Fig. 6 (TCP50H40), it can be seen that the distance between the base of the cones is similar to the distance between the base of the cylindrical pillars with a pitch of 30 μm (PP30H40). Accordingly, the
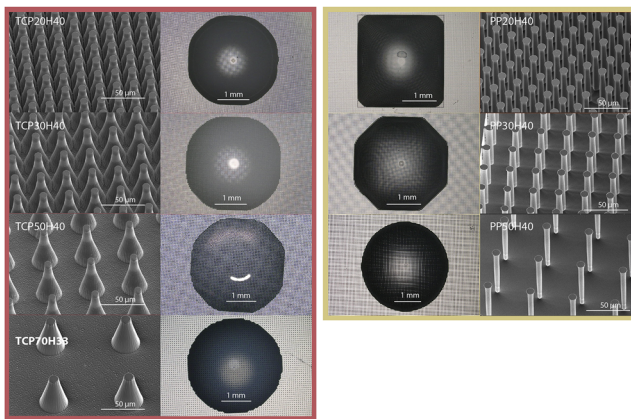
FIG. 6. Effect of the pitch distance of structures on the droplet shape. Both conical and cylindrical pillars have a height of H = 40 μm for a pitch range of 20–50 μm. The droplets were deposited from a height of 2 cm (We = 12).

droplet shape over conical pillars with a pitch of 50 μm is octagonal and similar to the droplet observed on cylindrical pillars for a pitch of 30 μm. In order to verify this, a droplet was deposited on a surface with conical pillars with a pitch of 70 μm, as shown in the last row of Fig. 6. Here, the distance from the cone base to the cone base is approximately the same as the pitch of 50 μm for cylindrical pillars in the same figure. In both cases, the droplet presents a round shape.

Since the difference between the droplet shape lying on cylindrical and conical pillars is attributed to the difference in capillary force acting in the normal and diagonal directions, we performed similar experiments for varying liquid surface tensions. Three ethanol/DI water mixtures were used (see Table II) with surface tension ranging from 27 to 37 mN/m. Figure 7 shows the droplets of the three mixtures lying on the surfaces with cylindrical and conical pillars. Note that the droplet of 37 mN/m in surface tension was no longer in a Wenzel wetting state so that surface tension could not be varied above this value for this study. Once again, the droplet shape is less rounded for the case of cylindrical pillars due to
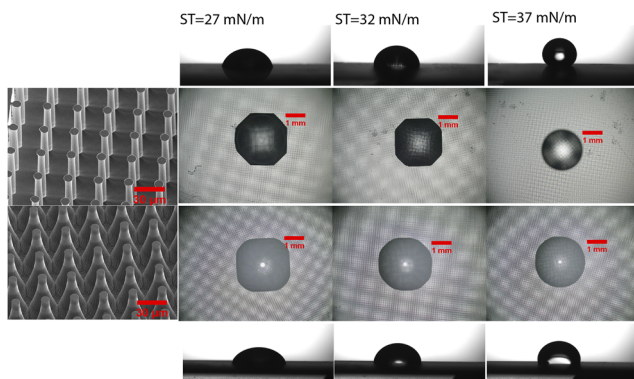
a larger anisotropy of the spreading velocity along the normal and diagonal directions to the row of pillars. As reported in a previous work,[13] as surface tension decreases, enhanced wettability helps to overcome the energy barrier needed for the depinning of the contact line, managing to keep a more square-like droplet shape.

In applications such as drop-on-demand inkjet printing, also seen as a manufacturing method with different materials,[30] the droplet is not gently deposited on the surface but rather impacts the surface with a certain speed V reaching up to around 10 m/s.[30] Therefore, in addition to capillary and viscous forces and pinning effects, inertia forces will also play an important role in the final

FIG. 7. Effect of surface tension for conical and cylindrical pillars of height H = 40 μm and pitch P = 30 μm. Droplets were deposited from a height of 1 cm (We = 6).
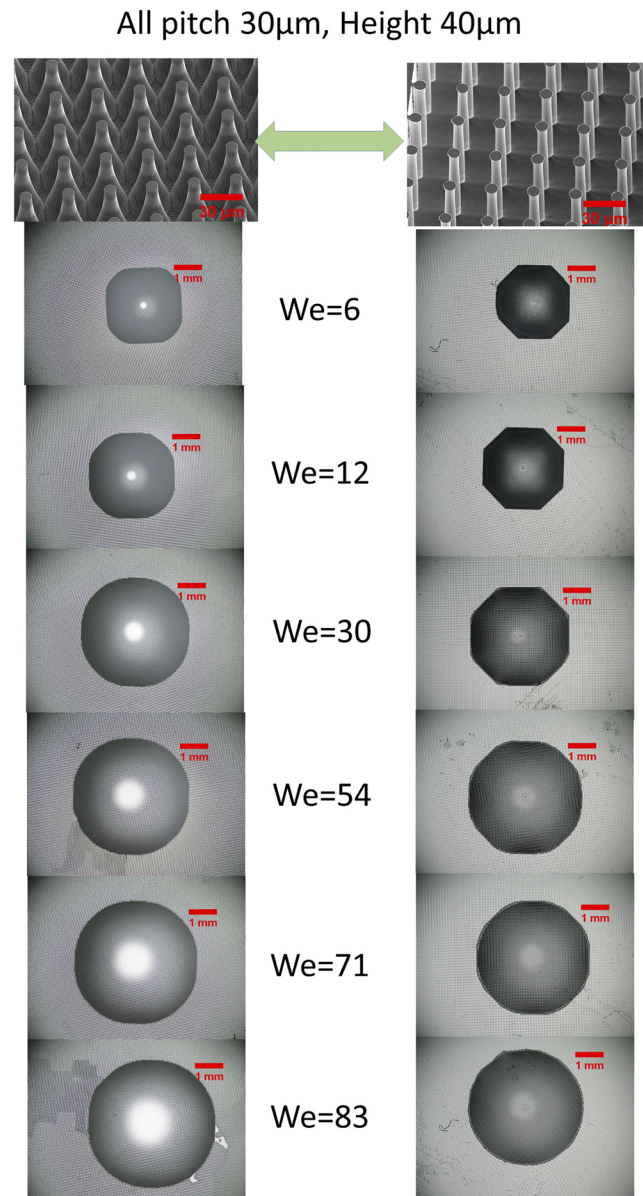
All pitch 30μm, Height 40μm

FIG. 8. Effect of impacting velocity on the droplet shape for conical (left) and cylindrical (right) pillars.

droplet shape. In this section, droplets were released from different heights ranging from 10 to 140 mm over cylindrical and conical pillar surfaces. The corresponding Weber number range is $6 < We < 83$, where $We = \rho R_{drop} V^2 / \gamma$, with ρ being the liquid density, R_{drop} being the droplet radius, V being the impact velocity obtained from the video imaging, and γ being the surface tension.

Figure 8 shows the effect of impacting velocity on the droplet shape over cylindrical and conical pillars. While anisotropic effects are evident for small We numbers, the droplets become rounded for higher impact velocities. In the case of cylindrical pillars, the droplet goes from an octagonal shape at low We numbers to a rounded droplet for $We > 54$. For the conical pillars, the droplet has the shape of a square with rounded corners for low We numbers, and it transitions to a rounded droplet already for $We > 30$.

When a droplet impacts on a surface, the spreading dynamics are initially governed by inertia forces until reaching the maximum spreading diameter, determined by capillary and viscous forces taking over inertia,[31] followed by the retracting regime. It has been pointed out that anisotropic spreading and faceted droplets will depend on We and topography characteristics for low We numbers.[27] In addition, during the droplet impact on a structured surface and depending on the We number, the liquid can penetrate the structures and may touch the bottom of the surface.[22,23,25] This implies that the liquid can move preferably above or within the structures, with the former occurring for lower impact We numbers. Once the maximum spreading diameter is reached, pinning effects will dominate the initiation of the retraction regime. The dissipation of energy will occur at the three-phase contact line pinned on the structures[27,32] due to the energy threshold to overcome pinning. The following droplet retraction process will depend on the surface wettability.[31,33] For superhydrophobic surfaces where Cassie droplets are observed, the faceted configuration of the triple line at the retraction stage[27] and the air below the droplet[23] have been attributed to the reason for the resulting droplet shape after the impact. As compared to Cassie state droplets, droplets in the Wenzel state show lower receding velocities due to the larger pinning force at the top of the structures.[24]

TABLE III. Patterned surfaces and impact conditions (droplet impact velocity or impact We number) from the literature and from this work.

Structure	Impact velocity (m/s)	We	Reference
Square post array	$\cdots$	19.4–79.0	Rhombus shape and rhombus shape with a branch at the corner. Liquid spreads both below and above the structure.[34]
Circular post square array	$\cdots$	$\cdots$	From a circular to a square shape when the defect size is increased.[12]
Circular post array	~2.0	$\cdots$	Shape is affected by surface tension or the aspect ratio.[13]
Square or hexagonal array	~6.0	~18.0	Droplet shape is affected by the pillar shape and pillar lattice design.[14]
Circular post array	$\cdots$	14.7	Pitch affects the droplet shape.[35]
Micropillar arrays in square, rectangular, and hexagonal patterns	$\cdots$	$\cdots$	Various droplet shapes are produced and attributed to the advancing behavior: Rectangles, hexagons, octagons, dodecagons, squares, and circles.[11]
Mesh surface	$\cdots$	$\cdots$	Liquid shape is affected by the injection rate and mesh layer placement.[36]
Square shape pillar array	$\cdots$	0.1	Droplet shape is affected by interfacial tension and the rough surface.[17]
Micro-pyramid array	$\cdots$	$\cdots$	Salt potassium chloride concentration can modify the droplet shape.[16]
Micro-pyramid cavity array	$\cdots$	$\cdots$	Ethanol concentration affects the droplet shape.[15]
Micro-pyramid array	$\cdots$	$\cdots$	Surfactant concentration affects the evaporating droplet shape.[37]
Quasi-periodic structure array	$\cdots$	10^{-6}	Surface topography and the self-similarity of the surface structure dominate droplet shape formation.[38]
Conical posts with nano-particles	$\cdots$	6.6–28.3	Heterogeneous shape during spreading/receding depends on the We number and structure array.[27]
Patterned microcavity arrays	$\cdots$	$<2.1 \times 10^{-5}$	Shape evolution is related to wetting state transition.[19]
Truncated cone or cylindrical pillar array	0.4–1.7	6.0–83.0	Droplet shape is also affected by the sidewall shape (this work).

For the droplets shown in Fig. 8, it is expected that the liquid manages to penetrate more into the conical structures than into the cylindrical pillars at lower We numbers, mainly due to the pinning of the liquid on the top of the cylindrical structures and inclined walls of the cones. In this case, the energy dissipation in the case of conical pillars is mainly due to viscous forces due to the larger liquid–solid contact area as compared to the pillars, whereas for the cylindrical pillars, the main dissipation mechanism is pinning on the top of the pillars. Since the pinning effect is assumed to be the reason for faceted droplets and anisotropic spreading velocities, this explains why the droplet on cylindrical pillars shows a polygonal shape at low We numbers. In the case of conical pillars, the viscous forces are dominant due to the partial penetration of the liquid and movement of the liquid within the structures. This viscous dissipation will dominate over capillary forces, reducing the anisotropy of spreading of the liquid in different directions at low We numbers. At higher We, the inertia force dominates over capillary and viscous forces and pinning effects, and the droplets show a circular shape for both cases.

In Table III, we summarize droplet impact conditions on structured surfaces from the literature[11,17,19,27,34–38] and from our work. Note that in many cases, not enough detailed conditions were given in the literature to estimate the corresponding We number. In this work, we cover a wider range of We numbers and reveal the effect of the structure sidewall shape on the final droplet shape, as compared to the straight lateral walls of the structures in the literature.

IV. CONCLUSIONS

In this work, we investigated faceted droplets after the impact on conical and cylindrical micropillars. Experiments were performed with three different mixtures of DI water and ethanol in order to vary the liquid surface tension, resulting in Wenzel state droplets for the tested surfaces. Impact velocities were varied between 0.4 and 1.7 m/s, with the corresponding Weber number range of $6 < We < 83$.

It was found that even at a constant height-to-pitch ratio of the structures and the same surface tension of the fluid, the droplet shape was different when lying on conical or cylindrical pillars. This shows that the lateral wall of the structures has a strong effect on the difference in liquid spreading velocities along the diagonal and normal directions to the structures. The liquid spreading is more anisotropic for the case of cylindrical pillars, resulting in polygonal-shaped droplets as opposed to more rounded droplets on the conical pillars. Due to the sidewall shape of the conical structures, viscous dissipation is much larger since the solid–liquid contact area is higher, whereas for cylindrical pillars, the dissipation occurs mainly on the pillar tops, thus resulting in a more faceted droplet. As the pitch increases, conical structures become far enough from each other so that the spreading of the liquid resembles the spreading between cylindrical pillars. We also show that the droplet can evolve into a more circular shape by increasing the impact velocity. Higher impact velocity allows the liquid to penetrate into the structures. The liquid moving above the structure is mainly inertia driven, while the liquid moving below and within the structures is affected by capillary and viscous forces. Pinning effects will be relevant in both cases.

AUTHOR DECLARATIONS

Conflict of Interest

The authors have no conflicts to disclose.

DATA AVAILABILITY

The data that support the findings of this study are available from the corresponding author upon reasonable request.

REFERENCES

[1]R. J. Good, "Contact angle, wetting, and adhesion: A critical review," J. Adhes. Sci. Technol. **6**, 1269–1302 (1992).

[2]D. Quéré, "Wetting and roughness," Annu. Rev. Mater. Res. **38**, 71–99 (2008).

[3]P. Calvert, "Inkjet printing for materials and devices," Chem. Mater. **13**, 3299–3305 (2001).

[4]J. Kettle, T. Lamminmäki, and P. Gane, "A review of modified surfaces for high speed inkjet coating," Surf. Coat. Technol. **204**, 2103–2109 (2010).

[5]S. Chen, M. Su, C. Zhang, M. Gao, B. Bao, Q. Yang, B. Su, and Y. Song, "Fabrication of nanoscale circuits on inkjet-printing patterned substrates," Adv. Mater. **27**, 3928–3933 (2015).

[6]B.-J. de Gans and U. S. Schubert, "Inkjet printing of well-defined polymer dots and arrays," Langmuir **20**, 7789–7793 (2004).

[7]B. K. Park, D. Kim, S. Jeong, J. Moon, and J. S. Kim, "Direct writing of copper conductive patterns by ink-jet printing," Thin Solid Films **515**, 7706–7711 (2007).

[8]C. Ladd, J.-H. So, J. Muth, and M. D. Dickey, "3D printing of free standing liquid metal microstructures," Adv. Mater. **25**, 5081–5085 (2013).

[9]Q. Liu and M. Orme, "High precision solder droplet printing technology and the state-of-the-art," J. Mater. Process. Technol. **115**, 271–283 (2001).

[10]Q. Liu, M. C. Leu, and M. Orme, "High precision solder droplet printing technology: Principle and applications," in *Proceedings of the International Symposium on Advanced Packaging Materials Processes, Properties and Interfaces* (IEEE, 2001), pp. 104–109.

[11]R. Raj, S. Adera, R. Enright, and E. N. Wang, "High-resolution liquid patterns via three-dimensional droplet shape control," Nat. Commun. **5**, 4975 (2014).

[12]T. Cubaud and M. Fermigier, "Faceted drops on heterogeneous surfaces," Europhys. Lett. **55**, 239 (2001).

[13]L. Courbin, E. Denieul, E. Dressaire, M. Roper, A. Ajdari, and H. A. Stone, "Imbibition by polygonal spreading on microdecorated surfaces," Nat. Mater. **6**, 661–664 (2007).

[14]R. J. Vrancken, M. L. Blow, H. Kusumaatmaja, K. Hermans, A. M. Prenen, C. W. M. Bastiaansen, D. J. Broer, and J. M. Yeomans, "Anisotropic wetting and de-wetting of drops on substrates patterned with polygonal posts," Soft Matter **9**, 674–683 (2013).

[15]H. Feng, K. S.-L. Chong, K.-S. Ong, and F. Duan, "Octagon to square wetting area transition of water–ethanol droplets on a micropyramid substrate by increasing ethanol concentration," Langmuir **33**, 1147–1154 (2017).

[16]X. Zhong, J. Ren, M. Lin, K. S. L. Chong, K.-S. Ong, and F. Duan, "Octagonal wetting interface evolution of evaporating saline droplets on a micropyramid patterned surface," ACS Appl. Mater. Interfaces **9**, 28055–28063 (2017).

[17]E. Chen, Q. Yuan, X. Huang, and Y.-P. Zhao, "Dynamic polygonal spreading of a droplet on a lyophilic pillar-arrayed surface," J. Adhes. Sci. Technol. **30**, 2265–2276 (2016).

[18]A. Kumar and R. Raj, "Droplets on microdecorated surfaces: Evolution of the polygonal contact line," Langmuir **33**, 4854–4862 (2017).

[19] W. Xu, Y. Liu, B. Xiao, H. Jiang, M. Chen, and Y. Wang, "Directional metastable wetting evolution of droplets on artificial patterned microcavity surfaces," Adv. Mater. Interfaces 8, 2100174 (2021).

[20] Y. Chen, B. He, J. Lee, and N. A. Patankar, "Anisotropy in the wetting of rough surfaces," J. Colloid Interface Sci. 281, 458–464 (2005).

[21] H. Ding and T. G. Theofanous, "The inertial regime of drop impact on an anisotropic porous substrate," J. Fluid Mech. 691, 546–567 (2012).

[22] L. Xu, "Liquid drop splashing on smooth, rough, and textured surfaces," Phys. Rev. E 75, 056316 (2007).

[23] M. Reyssat, D. Richard, C. Clanet, and D. Quéré, "Dynamical superhydrophobicity," Faraday Discuss. 146, 19–33 (2010).

[24] D. Li, G. S. Wu, G. Wang, Y. D. Wang, D. Liu, D. C. Zhang, Y. F. Chen, G. P. Peterson, and R. Yang, "Enhancing flow boiling heat transfer in microchannels for thermal management with monolithically-integrated silicon nanowires," Nano Lett. 12, 3385–3390 (2012).

[25] C. Guo, D. Zhao, Y. Sun, M. Wang, and Y. Liu, "Droplet impact on anisotropic superhydrophobic surfaces," Langmuir 34, 3533–3540 (2018).

[26] V. Vaikuntanathan and D. Sivakumar, "Maximum spreading of liquid drops impacting on groove-textured surfaces: Effect of surface texture," Langmuir 32, 2399–2409 (2016).

[27] J. Su, I. Legchenkova, C. Liu, C. Lu, G. Ma, E. Bormashenko, and Y. Liu, "Faceted and circular droplet spreading on hierarchical superhydrophobic surfaces," Langmuir 36, 534 (2020).

[28] T. Homola, L. Y. L. Wu, and M. Černák, "Atmospheric plasma surface activation of poly(ethylene terephthalate) film for roll-to-roll application of transparent conductive coating," J. Adhes. 90, 296–309 (2014).

[29] J. Kim, M.-W. Moon, and H.-Y. Kim, "Dynamics of hemiwicking," J. Fluid Mech. 800, 57–71 (2016).

[30] B. Derby, "Inkjet printing of functional and structural materials: Fluid property requirements, feature stability, and resolution," Annu. Rev. Mater. Res. 40, 395–414 (2010).

[31] A. L. Yarin, "Drop impact dynamics: Splashing, spreading, receding, bouncing. . .," Annu. Rev. Fluid Mech. 38, 159–192 (2006).

[32] H. Park, W. W. Carr, J. Zhu, and J. F. Morris, "Single drop impaction on a solid surface," AIChE J. 49, 2461–2471 (2003).

[33] M. Lee, Y. S. Chang, and H.-Y. Kim, "Drop impact on microwetting patterned surfaces," Phys. Fluids 22, 072101 (2010).

[34] D. Sivakumar, K. Katagiri, T. Sato, and H. Nishiyama, "Spreading behavior of an impacting drop on a structured rough surface," Phys. Fluids 17, 100608 (2005).

[35] X. Li, L. Mao, and X. Ma, "Dynamic behavior of water droplet impact on microtextured surfaces: The effect of geometrical parameters on anisotropic wetting and the maximum spreading diameter," Langmuir 29, 1129–1138 (2013).

[36] H. Kim, Z. Zheng, and H. A. Stone, "Noncircular stable displacement patterns in a meshed porous layer," Langmuir 31, 5684–5688 (2015).

[37] X. Zhong, J. Ren, K. S.-L. Chong, K.-S. Ong, and F. Duan, "Controlling octagon-to-square wetting interface transition of evaporating sessile droplet through surfactant on microtextured surface," ACS Appl. Mater. Interfaces 10, 11425–11429 (2018).

[38] C. A. Chen, T. F. Lin, W.-M. Yan, and M. Amani, "Time periodic evaporation heat transfer of R-134a in a narrow annular duct due to mass flow rate oscillation," Int. J. Heat Mass Transfer 118, 154–164 (2018).